Theor Chem Acc (2001) 105:173–181
DOI 10.1007/s002140000197

Theoretical
Chemistry Accounts

Regular Article

Dual propagation inversion of truncated signals

David K. Hoffman[1], **Hongzhen Zhang**[2], **Zhuoer Shi**[2], **Donald J. Kouri**[2], **Sungyul Lee**[3], **Eli Pollak**[4]

[1] Department of Chemistry and Ames Laboratory, Iowa State University, Ames, IA 50011, USA
[2] Department of Physics and Department of Chemistry, University of Houston, Houston, TX 77204, USA
[3] Department of Chemistry, Kyunghee University, Kyungki-do 449–701, Korea
[4] Chemical Physics Department, Weizman Institute of Science, Rehovot 76100, Israel

Received: 30 January 2000 / Accepted: 6 July 2000 / Published online: 23 November 2000

Abstract. Fourier transforms occur in a variety of chemical systems and processes. A few examples include obtaining spectral information from correlation functions, energy relaxation processes, spectral densities obtained from force autocorrelation functions, etc. In this article, a new functional transform, named the dual propagation inversion (DPI) is introduced. The DPI functional transform can be applied to a variety of problems in chemistry, such as Fourier transforms of time correlation functions, energy relaxation processes, rate theory, etc. The present illustrative application is to generating the frequency representation of a discrete, truncated time-domain signal. The DPI result is compared with the traditional Fourier transform applied to the same truncated time signal. For both noise-free and noise-corrupted time-truncated signals, the DPI spectrum is found to be more accurate, particularly as the signal is more severely truncated. In the DPI, the distributed-approximating-functional free propagator is used to propagate and denoise the signal simultaneously.

Key words: Dual propagation inversion – Distributed approximating functional – Fourier transform – Time correlation function – Denoise

1 Introduction

In a variety of physics, chemistry and engineering contexts, it is common to require the transformation of information from a ''physical'' domain to a complementary domain. This generally involves the evaluation of a function transform of the form

$$G(t) = \int_{-\infty}^{\infty} K(t,\omega)g(\omega)\mathrm{d}\omega \ , \tag{1}$$

where $K(t,\omega)$ is called the ''transform kernel''. The quantities t and ω are known as conjugate variables. Extracting the information represented by $g(\omega)$ from $G(t)$ is referred to as an ''inversion''. Important examples of the inversion problem are provided by Fourier and Laplace transforms. Such transforms are ubiquitous in chemistry. Some examples include the evaluation of molecular spectra by Fourier transform of time correlation functions [1], energy relaxation processes [2, 3], spectral densities by Fourier transform of force autocorrelation functions [4], Wigner distribution functions in multidimensional systems [5], reaction rate constants [6], absorption or Raman spectra from autocorrelation functions [7] and extraction of vibrational frequencies from a molecular-dynamics-simulated time signal [8]. From experimental or computational studies, the $G(t)$ function value is typically known only on a finite, discrete set of points. Although a formal analytical result may be obtained by directly applying the appropriate mathematical inversion of the analytical function, $G(t)$, one generally faces serious difficulties in numerically determining the value of $g(\omega)$ from a finite number of $G(t)$ values. Additionally, noise is generally always present in the measured data. In the Laplace transform, the inversion is typically unstable owing to amplification of noise contained in measured $G(t_i)$ data [9]. Inverse Fourier transforms yield low-resolution spectra and low accuracy for low-frequency processes when a time signal of sufficiently long duration is not available [10, 11].

In this article, we describe a new procedure for numerically inverting such an integral equation. This method, which we term the ''dual propagation inversion'' (DPI), makes use of the distributed-approximating-functional (DAF) free propagator [12] to carry out the inversion (but other numerical techniques such as the fast Fourier transform [13, 14] may also be used). The DPI method can be applied to many physical conjugate–variable transforms such as energy–temperature transforms, etc. We shall frame our discussion in the context of time- and frequency-domain signals. The time-domain signal and the frequency-domain spectrum are related by the Fourier transform

$$G(t) = \int_{-\infty}^{\infty} \mathrm{d}\omega \ \exp(-i\omega t)g(\omega) \tag{2}$$

and its inverse

$$g(\omega) = \frac{1}{2\pi} \int_{-\infty}^{\infty} \mathrm{d}t \ \exp(i\omega t) G(t) \ . \tag{3}$$

One difficulty in the direct inversion by Eq. (3) is that, in order to resolve low-frequency features, one needs to know the autocorrelation function (time signal) for a long duration. When the signal is available only on a set of discrete times and for too short a time period, the direct Fourier transform becomes inaccurate. Several elegant methods, such as the filter-diagonalization techniques, developed by Neuhauser [15] and modified by Mandelshtam and Taylor [16], have been proposed for such problems. Ours is an alternative approach.

2 Theory

In the present DPI approach, a factor $\exp\left[i\alpha(\omega-\omega_0)^2\right]$ is inserted into Eq. (2), and an auxiliary function is defined as

$$\tilde{g}(t,\alpha,\omega_0) = \int_{-\infty}^{\infty} \mathrm{d}\omega \ \exp\left[i\alpha(\omega-\omega_0)^2\right] \exp(-i\omega t) g(\omega) \ . \tag{4}$$

It is well known that

$$\exp\left[i\alpha(\omega-\omega_0)^2\right] = \left(\frac{\pi i}{\alpha}\right)^{\frac{1}{2}} \left\langle \omega \left| \exp\left(\frac{i}{4\alpha}\frac{\mathrm{d}^2}{\mathrm{d}\omega^2}\right) \right| \omega_0 \right\rangle \ , \tag{5}$$

so the factor $\exp\left[i\alpha(\omega-\omega_0)^2\right]$ can be interpreted as a matrix element of the "free propagator" $\exp\left(\frac{i}{4\alpha}\frac{\mathrm{d}^2}{\mathrm{d}\omega^2}\right)$, acting on $\exp(-i\omega t)g(\omega)$. Therefore, the integration over ω in Eq. (4) is equivalent to evaluating the action of $\exp\left(\frac{i}{4\alpha}\frac{\mathrm{d}^2}{\mathrm{d}\omega^2}\right)$ in the continuous "ω" representation and the introduction of the phase $[i\alpha(\omega-\omega_0)]^2$ is equivalent to freely propagating $\exp(-i\omega t)g(\omega)$ up to the generalized time of $1/(4\alpha)$. Henceforth, we use the term "duration". This enables us to write Eq. (4) as

$$\tilde{g}(t;\alpha,\omega_0) = \left(\frac{\pi i}{\alpha}\right)^{\frac{1}{2}} \left\{ \exp\left(\frac{i}{4\alpha}\frac{\mathrm{d}^2}{\mathrm{d}\omega^2}\right) [\exp(-i\omega t) g(\omega)] \right\} \Bigg|_{\omega=\omega_0}^{t} . \tag{6}$$

The function $g(\omega)$ is then obtained simply by inverting Eq. (6),

$$g(\omega_0) = \left(\frac{\alpha}{\pi i}\right)^{\frac{1}{2}} \exp(i\omega_0 t) \exp\left(-\frac{i}{4\alpha}\frac{\mathrm{d}^2}{\mathrm{d}\omega_0^2}\right) \tilde{g}(t;\alpha,\omega_0) \ . \tag{7}$$

$g(\omega)$ is the same as $g(\omega_0)$, where we choose ω_0 to equal whatever value of frequency ω we desire.

For this Eq. (7) to be of any use, we need an independent method for calculating the auxiliary function from the experimentally (or numerically) determined $G(t)$. Next, we shall show how to calculate $\tilde{g}(t;\alpha,\omega_0)$ from $G(t)$. Define

$$\tilde{h}(t;\alpha,\omega_0) \equiv \exp(i\omega_0 t)\tilde{g}(t;\alpha,\omega_0) \ . \tag{8}$$

According to Eq. (4), Eq. (8) can be rewritten as

$$\tilde{h}(t;\alpha,\omega_0) = \int \mathrm{d}\omega \ \exp\left[i\alpha(\omega-\omega_0)^2\right] \exp[-i(\omega-\omega_0)t] g(\omega) \ . \tag{9}$$

By performing a partial derivative with respect to α on Eq. (9) and two partial derivatives with respect to t on Eq. (9), respectively, we obtain

$$\frac{\partial}{\partial\alpha}\tilde{h}(t;\alpha,\omega_0) = \int \mathrm{d}\omega \ i(\omega-\omega_0)^2 \ \exp\left[i\alpha(\omega-\omega_0)^2\right] \times \exp[-i(\omega-\omega_0)t] g(\omega) \tag{10}$$

and

$$\frac{\partial^2}{\partial t^2}\tilde{h}(t;\alpha,\omega_0) = \int \mathrm{d}\omega \ i^2(\omega-\omega_0)^2 \ \exp\left[i\alpha(\omega-\omega_0)^2\right] \times \exp[-i(\omega-\omega_0)t] g(\omega) \ . \tag{11}$$

From Eqs. (10) and (11), it follows that

$$\frac{\partial}{\partial\alpha}\tilde{h}(t;\alpha,\omega_0) = -i\frac{\partial^2}{\partial t^2}\tilde{h}(t;\alpha,\omega_0) \ . \tag{12}$$

This has the same form as the free particle time-dependent Schrödinger equation, whose propagator is known:

$$\tilde{g}(t;\alpha,\omega_0) = \exp(-i\omega_0 t) \exp\left(-i\alpha\frac{\mathrm{d}^2}{\mathrm{d}t^2}\right) [\exp(i\omega_0 t) G(t)] \ . \tag{13}$$

Note that $[\exp(i\omega_0 t)G(t)]$ is a frequency-modulated time signal. In signal processing, the effect of the modulation factor $\exp(i\omega_0 t)$ is to translate the spectrum of the signal $G(t)$ by an amount ω_0. The frequency ω_0 and "duration" α are parameters which can be chosen for numerical convenience. Thus, our procedure is, first, to propagate freely the frequency-modulated signal $[\exp(i\omega_0 t)G(t)]$ in the time domain over a "duration" of α to obtain $\tilde{g}(t;\alpha,\omega_0)$ and, second, to propagate the resulting $\tilde{g}(t_0;\alpha,\omega_0)$ in the frequency domain over the duration of $1/(4\alpha)$. Note that the product of the two propagation "durations" is a constant $\alpha \times \frac{1}{4\alpha} = \frac{1}{4}$ and, therefore, obeys a "time-energy"-like uncertainty principle. For numerical convenience, we choose $\alpha = 1/2$.

The DAF free propagator is used to perform the two propagations. In actual computations, the discretized version of the DAF free propagator is applied. In the first propagation, Eq. (13) becomes [12, 18]

$$\tilde{g}(t;\alpha,\omega_0) = \exp(-i\omega_0 t) \sum_{k=-\infty}^{\infty} F[t,t_k|M,\sigma(0),\Delta t,\alpha] \times [\exp(i\omega_0 t_k) G(t_k)] \ , \tag{14}$$

where

$$F(t,t_k|M,\sigma(0),\Delta t,\alpha)=\Delta t\sum_{n=0}^{M/2}b_n\left(\frac{\sigma(0)}{\sigma(\alpha)}\right)^{2n+1}\times\exp\left(-\frac{(t-t_k)^2}{2\sigma(\alpha)^2}\right)\times H_{2n}\left(\frac{(t-t_k)}{\sqrt{2}\sigma(\alpha)}\right)\ , \tag{15}$$

$$b_n=(-1)^n\Big/\left[(2\pi)^{\frac{1}{2}}\sigma(0)n!2^{2n}\right]\ , \tag{16}$$

The second propagation (Eq. 7) can be done analytically; however, for numerical convenience, we chose to follow a procedure analogous to the first propagation, so

$$g(\omega_{0p})=\exp(i\omega_0 t_c)\sum_{q=-\infty}^{\infty}F\left[\omega_{0p},\omega_{0q}|M,\sigma(0),\Delta\omega_0,\alpha\right]\times\left\{\tilde{g}(t_c;\alpha,\omega_{0q})\right\} \tag{17}$$

$$F\left[\omega_{0p},\omega_{0q}|M,\sigma(0),\Delta\omega_0,\alpha\right]=\Delta\omega_0\sum_{n=0}^{M/2}b_n\left(\frac{\sigma(0)}{\sigma(\alpha)}\right)^{2n+1}\times\exp\left(-\frac{(\omega_{0p}-\omega_{0q})^2}{2\sigma(\alpha)^2}\right)H_{2n}\left(\frac{(\omega_{0p}-\omega_{0q})}{\sqrt{2}\sigma(\alpha)}\right)\ . \tag{18}$$

In these equations, $\sigma(0)$ and M are DAF parameters, the H_{2n} are the even Hermite polynomials [12, 18], Δt is the time-grid interval and $\Delta\omega_0$ is the frequency-grid interval. The time t_c is arbitrary (i.e., the result is independent of t_c) if the procedure is carried out exactly using Eqs. (7) and (13). If the DAF approximation is "good", then the result depends only weakly on t_c. As noted later, in all computations, we set $t_c\equiv 0$. In the first propagation $\sigma^2(\alpha)=\sigma^2(0)+2i\alpha$ and in the second propagation $\sigma^2(\alpha)=\sigma^2(0)+i(1/2\alpha)$. For numerical convenience, we may choose $\alpha=1/2$, so $\sigma^2(\alpha)=\sigma^2(0)+i$ in both propagations. Since the signals of interest are finite (truncated), the range of the summation index k in Eq. (16) or q in Eq. (19) extends from the left-most grid point to the right-most grid point. Note that by using matrix products, one can write the two propagations as a single matrix operation, but this is not done here for clarity of presentation.

3 Model calculation

In actual experimental measurements, the time signal always has a finite duration, or "compact support". Similarly, one extracts a spectrum only over a finite range of frequency. However, compact support in the frequency domain implies an infinite data sequence in the time domain, and vice versa. As a result, one is always faced with aliasing [19] effects in signal analysis. Here we show that the DPI method is robust for processing a short-length, discretized data sequence. We compare the result with the spectrum obtained by the usual discrete Fourier transform. Both generate aliasing in the inverted spectrum.

The model signal we consider to test the DPI method is

$$g(\omega)=\begin{cases}\sin(\omega) & 0\le\omega\le\pi\\ 0 & \text{otherwise}\end{cases} \tag{19}$$

Although this may seem to be a simple spectrum, the occurrence of a discontinuity in the first derivative at $\omega=0,\ \pi$, causes the signal to "ring" for long times in the physical domain. Truncation of the time domain signal poses a significant challenge for Fourier inversion aliasing. The compact support model spectrum, $g(\omega)$, is shown in Fig. 1. Its time-domain representation, $G(t)$, is easily found analytically using Eq. (2), yielding

$$G(t)=\frac{1+\cos(t\pi)}{1-t^2}+i\frac{-\sin(t\pi)}{1-t^2}\quad -\infty<t<\infty \tag{20}$$

As pointed out earlier, it has slowly decaying behavior as a function of time. In our numerical simulation, the signal $G(t)$ is replaced by a finite set of function values, so the signal is truncated and discretized. The sampling interval used here is $\Delta t=0.05$. Similarly, our DAF free propagator is also discretized in ω_0, with a sampling grid spacing $\Delta\omega_0=0.05$. By Eq. (16), a discretized version of $\tilde{g}(t;\alpha,\omega_0)$, the auxiliary function, is obtained. Note that $\tilde{g}(t;\alpha,\omega_0)$ is a function of time, t, propagation duration, α, and auxiliary frequency variable, ω_0. The auxiliary function is propagated in the frequency domain by Eq. (7). We note that the auxiliary variable t is formally eliminated as a result of the second propagation. As mentioned earlier, t is, in principle, arbitrary, but numerically we found that use of $t=0$ yields reliable results. The first propagation duration, α, must be chosen consistent with the second propagation duration, $1/4\alpha$, in the complementary domain. A shorter propagation duration in one domain implies a longer propagation duration in the complementary domain. Thus, after the two free propagations, $g(\omega)$, the spectrum of the truncated, discretely sampled time signal, $G(t)$, is obtained. To verify the DPI approach to inverting a time

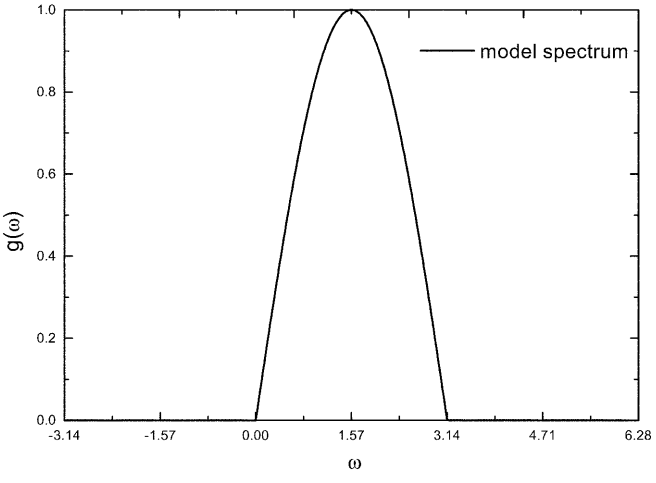

Fig. 1. Model spectrum

signal, we compare the resulting DPI spectrum with the exact result and that obtained using a standard Fourier transform for several truncated discretizations of the model signal, Eq. (22). The Fourier transform is applied by a periodic extension of the truncated, discretized time signal.

3.1 Model calculation on a slowly decaying, truncated signal

In this calculation, the DAF parameters were $M=40$ and $\sigma(0)/\Delta=2.5$ for both free propagations. A relatively long data sequence is generated by discretely sampling the continuous time signal $G(t)$ from $t=-45$ to 45. This truncated version of $G(t)$ is shown in Fig. 2. The sampling interval $\Delta t=0.05$ is short enough to satisfy the Nyquist [19] condition. The spectrum produced by the DPI is shown in Fig. 3 and the spectrum generated from the same data by the Fourier transform is shown in Fig. 4. We see from Figs. 3 and 4 that for this case the two methods yield visibly indistinguishable and highly accurate spectra differing from the exact spectrum only near the discontinuities in the derivative of the original spectrum. Both the DPI and Fourier transform produce the same slight amount of visibly observable aliasing near $\omega=0$ and $\omega=\pi$. Because the time duration is sufficiently long, the inverted signal has almost all of the original signal energy in the correct frequency regime.

3.2 Model calculation on noise-free and noise-corrupted short-time truncated signal

In the calculation described in Sect. 3.1, the truncated time signal is sufficiently long and has decayed close enough to zero, so one does not see large effects of truncation with either the DPI or the Fourier transform. As is standard in signal processing theory, a truncated signal can be taken as equivalent to the product of the original signal and a square window, where the width of the square window is just the truncated signal duration.

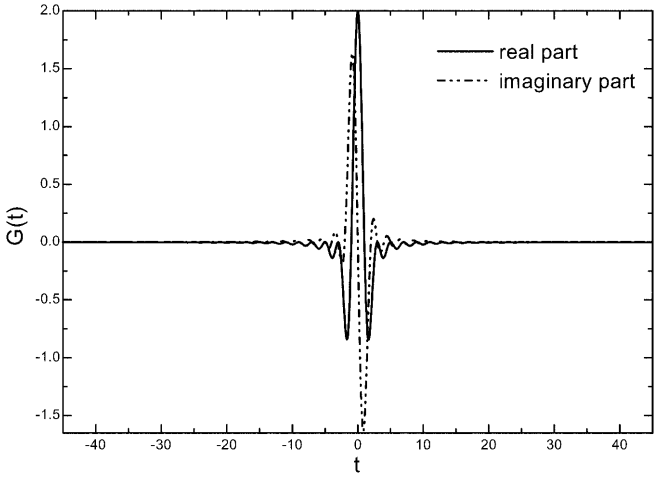

Fig. 2. (–45, 45) truncated time signal $G(t)$

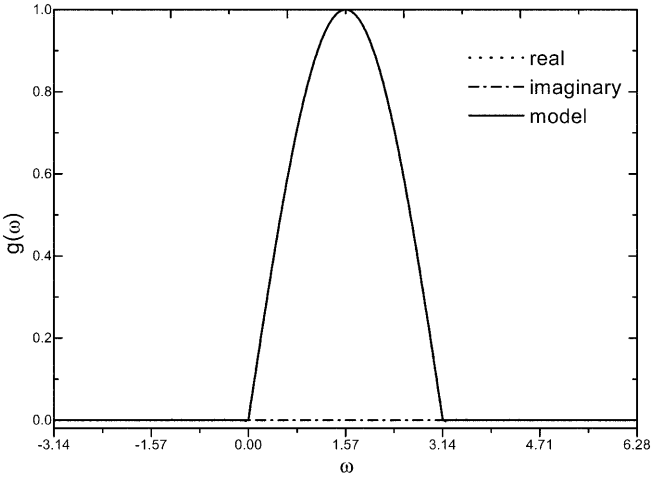

Fig. 3. Spectrum by dual propagation inversion (*DPI*). [Distributed-approximating-functional (*DAF*) parameter $M=40$, $\sigma(0)/\Delta)=2.5$]

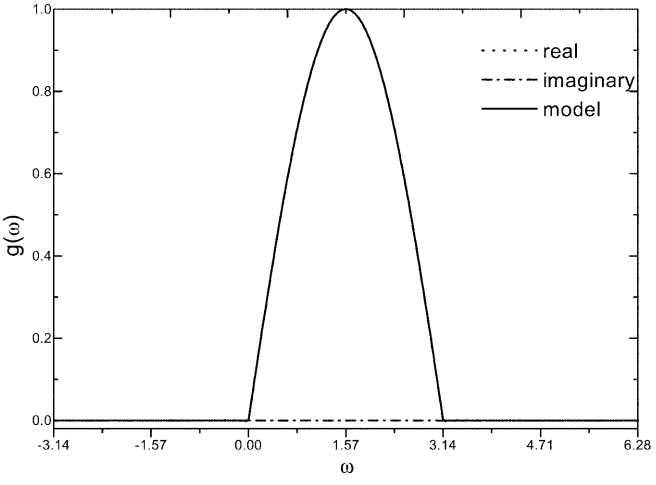

Fig. 4. Spectrum by Fourier transform

Since the Fourier transform of a square window is a sin C function, generally the decay will be proportional to $1/t$. In the present case, the window coincides with the nodes of the signal, so the discontinuity does not occur until the first derivative. This causes a faster $1/t^2$ decay for the model signal. In the time domain, we are using a square window that creates a discontinuity in the function itself. The result is a slow decay for the inverted signal for both the DPI and the Fourier inversion. Under noise-free conditions, it is the truncation by the square window that produces the spectrum distortion, known as the Gibbs effect. In our second model calculation, we consider the DPI spectrum resulting from a much shorter time signal, one which is one-ninth of the signal duration used in the calculation described in Sect. 3.1. The time signal in the new truncated range from -5 to 5 is shown in Fig. 5. The sampling interval is again $\Delta t=0.05$. The DPI result is shown in Fig. 6 and the Fourier transform result is shown in Fig. 7. Both are compared to the exact model spectrum and one can see

significant differences between the DPI and the Fourier transform. The real part of the DPI spectrum is visibly closer to the model spectrum in the compact region between 0 and π, except near the boundaries 0 and π. Thus, the DPI does better at reproducing the model spectrum in the true signal region. The Fourier transform loses energy near $\omega = \pi/2$, where the highest values of the model spectrum occur. Another interesting feature is that the real part of the DPI spectrum decreases faster than that of the Fourier transform outside the region $0 \le \omega \le \pi$. Even though both the DPI and the Fourier spectra exhibit aliasing, the faster DPI decay outside the true spectrum region is closer to the ideal compact support spectrum; however, the imaginary part of the DPI spectrum is slightly worse than that of the Fourier transform spectrum.

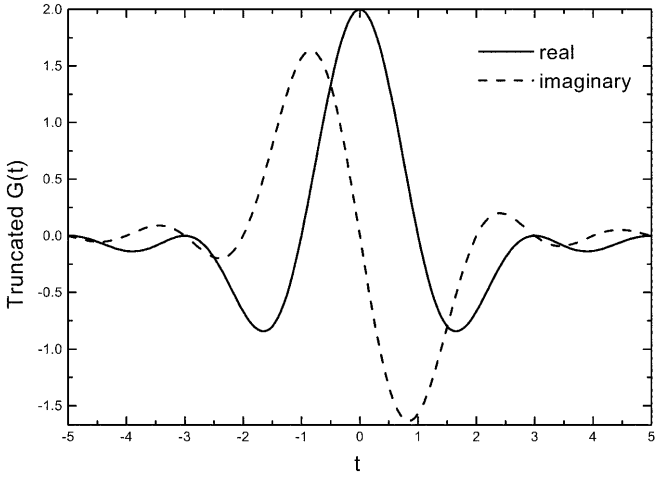

Fig. 5. (−5, 5) truncated time signal $G(t)$

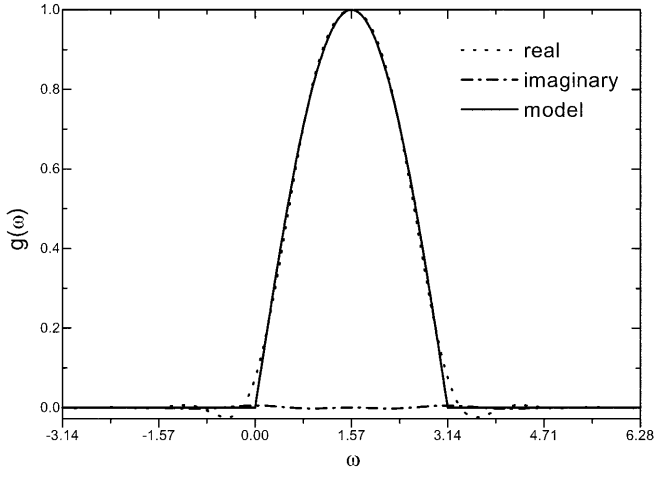

Fig. 6. Spectrum by DPI [time duration (−5, 5), DAF parameter $M = 6$, $\sigma(0)/\Delta = 10$]

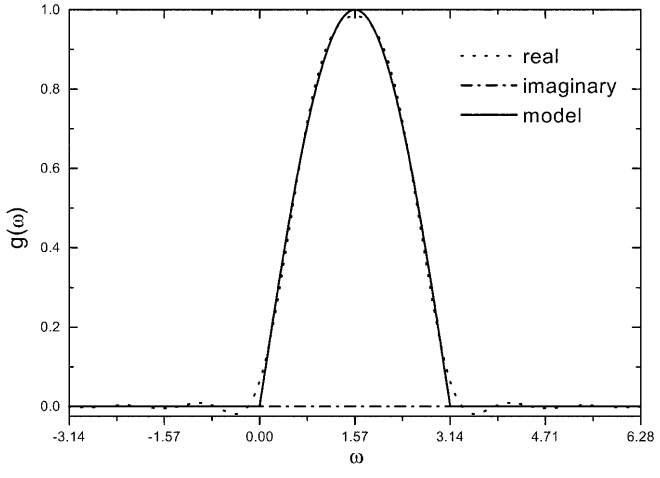

Fig. 7. Spectrum by Fourier transform [time duration (−5, 5)]

A more interesting test of the DPI is for a noise-corrupted time signal. It is well known [17] that the Hermite DAF is a low-pass filter. Since the Hermite DAF is just a special case of the DAF free propagator for a vanishing duration, the DAF free propagator behaves similarly in removing high-frequency noise. We plot in Fig. 8 the spectrum of the DAF free propagator, showing that it will filter out high-frequency components associated with noise.

A time signal truncated from −5 to 5 with 20% random noise is shown in Fig. 9. The computed DPI spectrum is shown in Fig. 10 and the Fourier transform spectrum is shown in Fig. 11. Because of noise corruption, the Fourier transform spectrum has significant distortion of both the real and imaginary parts. Under the same noise conditions, the DPI spectrum is more stable and its real part still closely tracks the model spectrum in the region $0 \le \omega \le \pi$. Additionally, the real part of the DPI spectrum decreases slightly faster to zero than the Fourier transform in the presence of noise. The DPI is very robust with respect to noise compared to the standard discrete Fourier transform. In the present case, the DAF parameters are $M = 6$, $\sigma(0)/\Delta = 11$ compared to the noise-free case values $M = 6$, $\sigma(0)/\Delta = 10$. Figure 8 shows that for a fixed M, increasing $\sigma(0)/\Delta$ shrinks the width of the low-pass filter and so more frequencies will be filtered out. This systematic behavior provides some guidance for choosing the DAF free propagator parameters combined with α to deal with a corrupted time signal.

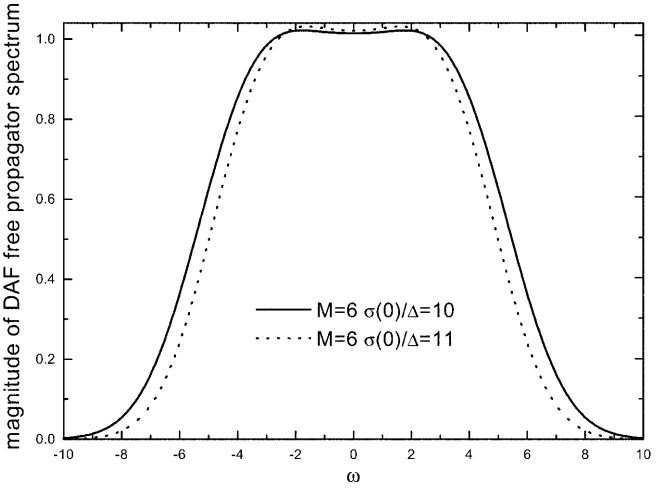

Fig. 8. Spectrum of DAF free propagator

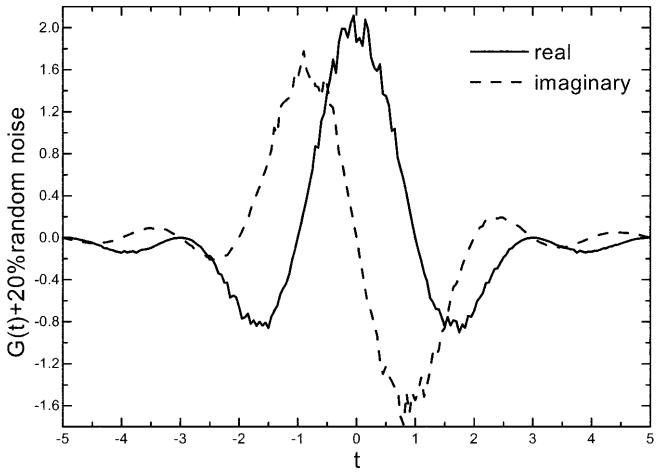

Fig. 9. 20% noise-corrupted time signal

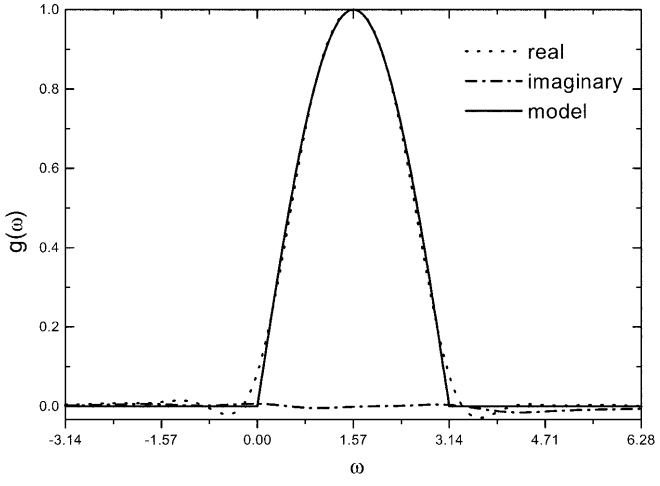

Fig. 10. Spectrum by DPI [time duration (−5, 5), +20% noise, DAF parameter $M=6$, $\sigma(0)/\Delta=11$]

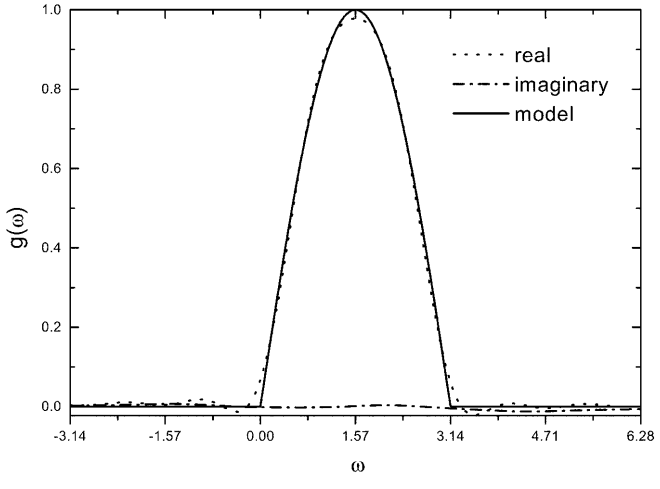

Fig. 11. Spectrum by Fourier transform [time duration (−5, 5), +20% noise]

3.3 Model calculation on noise-free and noise-corrupted short-time signal with padding

One technique to reduce aliasing further is to connect the truncated signal to some decaying function. The "padded" signal will then decay to zero more smoothly, giving rise to a smaller Gibbs effect and less distortion in the physical region of compact support. Optimally, the added tail should simulate the original signal as closely as possible, in order to produce the least distortion. In the present study, we employ an exponentially decaying tail, given by

$$g(t) = -0.04\exp(-0.1|t|) \qquad |t| > 7 \ . \tag{23}$$

The tail is reasonably good for replacing the infinite signal segment that has been cut off (although from Eq. 22, it clearly dies off too rapidly). To ensure the smoothness of the modified signal, a new technique called DAF padding [17] is applied. One assumes a gap between the known signal data and a region where the discretized signal values are determined by the tail function. The unknown discrete values in the gap are obtained by solving linear algebraic equations, resulting in a least-squares optimized DAF fit of the known and unknown data.

For this calculation, we first use DAF padding to fill the gaps between the noise-free truncated time signal located between $t=-5$ and $t=5$ and the artificial tail for $|t|>7$. The resultant signal waveform is shown in Fig. 12a. The gap detail is shown in Fig. 12b and c. As shown in Fig. 12b and c, the DAF padding supplies the gap values between |5| and |7|, which are based on the known signal information and the assumed tail. Compared to Fig. 2, we see that the main change in the padded signal and the true one is the more rapid decay to zero imposed by Eq. (23).

By applying both the DPI and Fourier transforms on the padded version of the discrete time signal, we obtain the spectrum shown in Fig. 13 for the DPI and Fig. 14 for the Fourier transform. Here the DAF parameters are $M=6$, $\sigma(0)/\Delta=9$. It is clear that the DPI spectrum is superior to that obtained by Fourier transform. The padded signal is, of course, not the same as the original signal and this is reflected in the fact that the Fourier transform is distorted both within and outside the compact support region. The DPI is not as sensitive to the detailed modification of the original data and yields a spectrum which still behaves correctly in most of the region $0 \le \omega \le \pi$; however, it also yields significantly less aliasing for $\pi < \omega < 0$ compared to the Fourier transform results in Fig. 14.

As previously discussed [17], DAF padding not only retains the basic information contained in the input, truncated signal, but also removes noise during the padding procedure. The tail was also DAF-padded to the 20% noise-corrupted signal (Fig. 9), where Fig. 15a shows the resultant time signal and Fig. 15b and c the padding detail. Figure. 15b and c shows that the padded signal between the known region and the exponential tail is smooth and similar to Fig. 12b and c, respectively. The resulting DPI and Fourier transform spectra are shown in Figs. 16 and 17, respectively. We see that the DPI

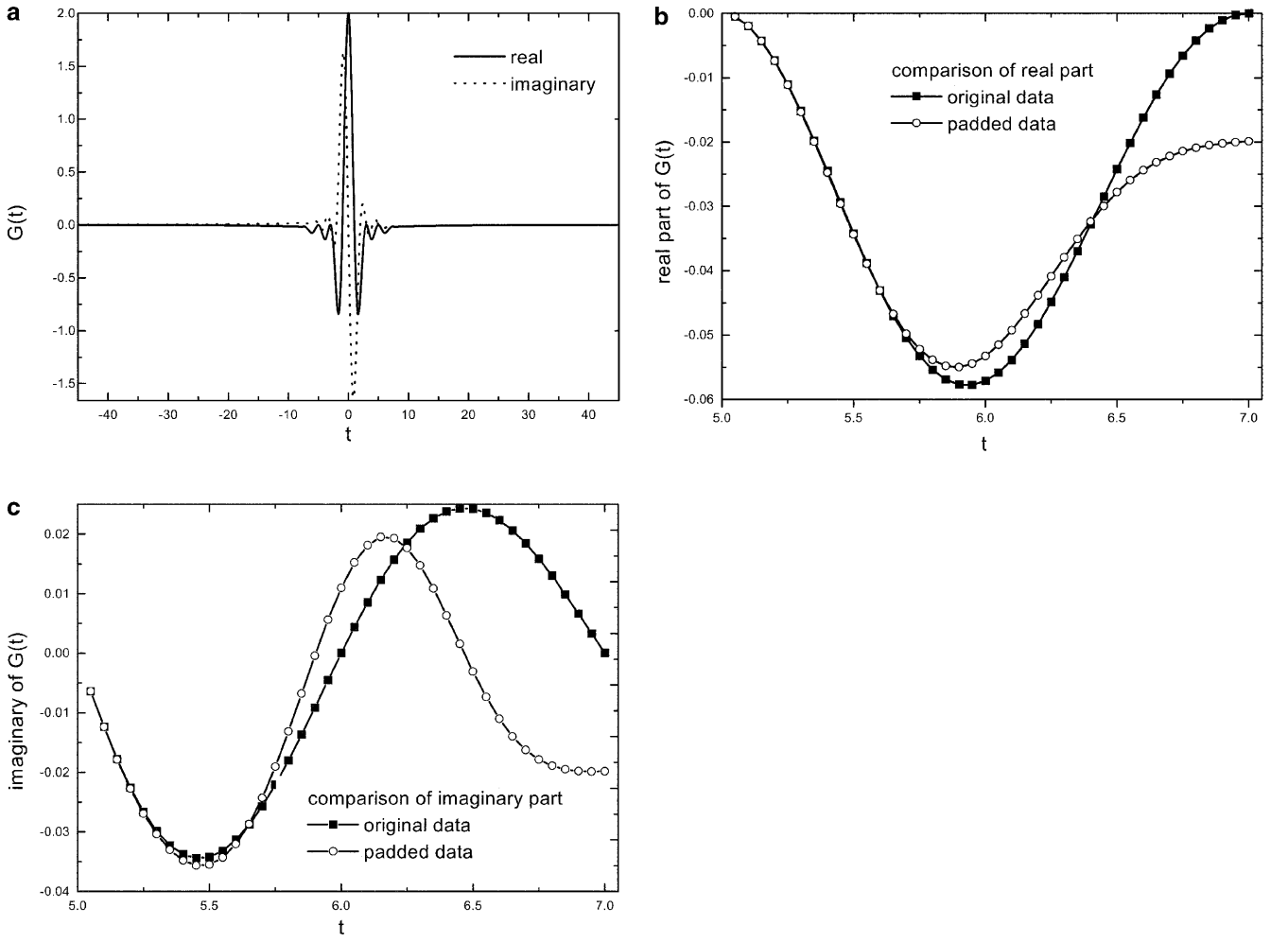

Fig. 12. **a** Time signal (DAF padding with exponential tail). **b** Real parts comparison of original and padded data in noise-free case. **c** Imaginary parts comparison of original and padded data in noise-free case

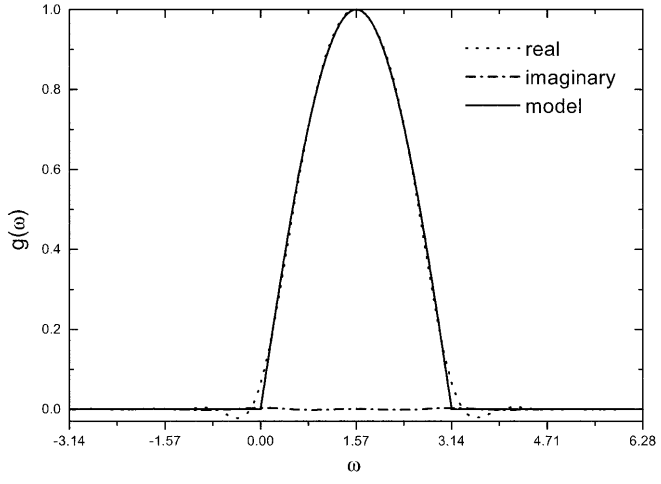

Fig. 13. Spectrum by DPI with DAF padding [DAF parameter $M=6$, $\sigma(0)/\Delta)=9$]

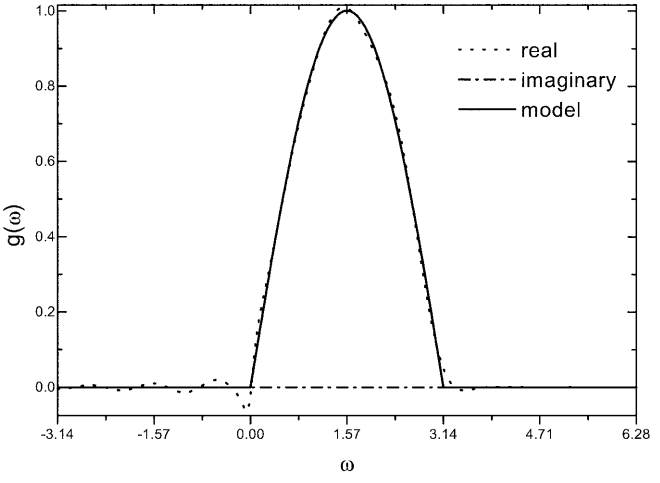

Fig. 14. Spectrum by Fourier transform (DAF padding)

procedure treats the noise very well while following the model spectrum closely in the compact support region and decreasing rapidly to zero outside that region. Here the DAF parameters are $M=6$, $\sigma(0)/\Delta=10$. The Fourier transform spectrum is strongly distorted relative to the model, showing greater sensitivity to the noise in the signal, the exponential tail and the padding gap. We

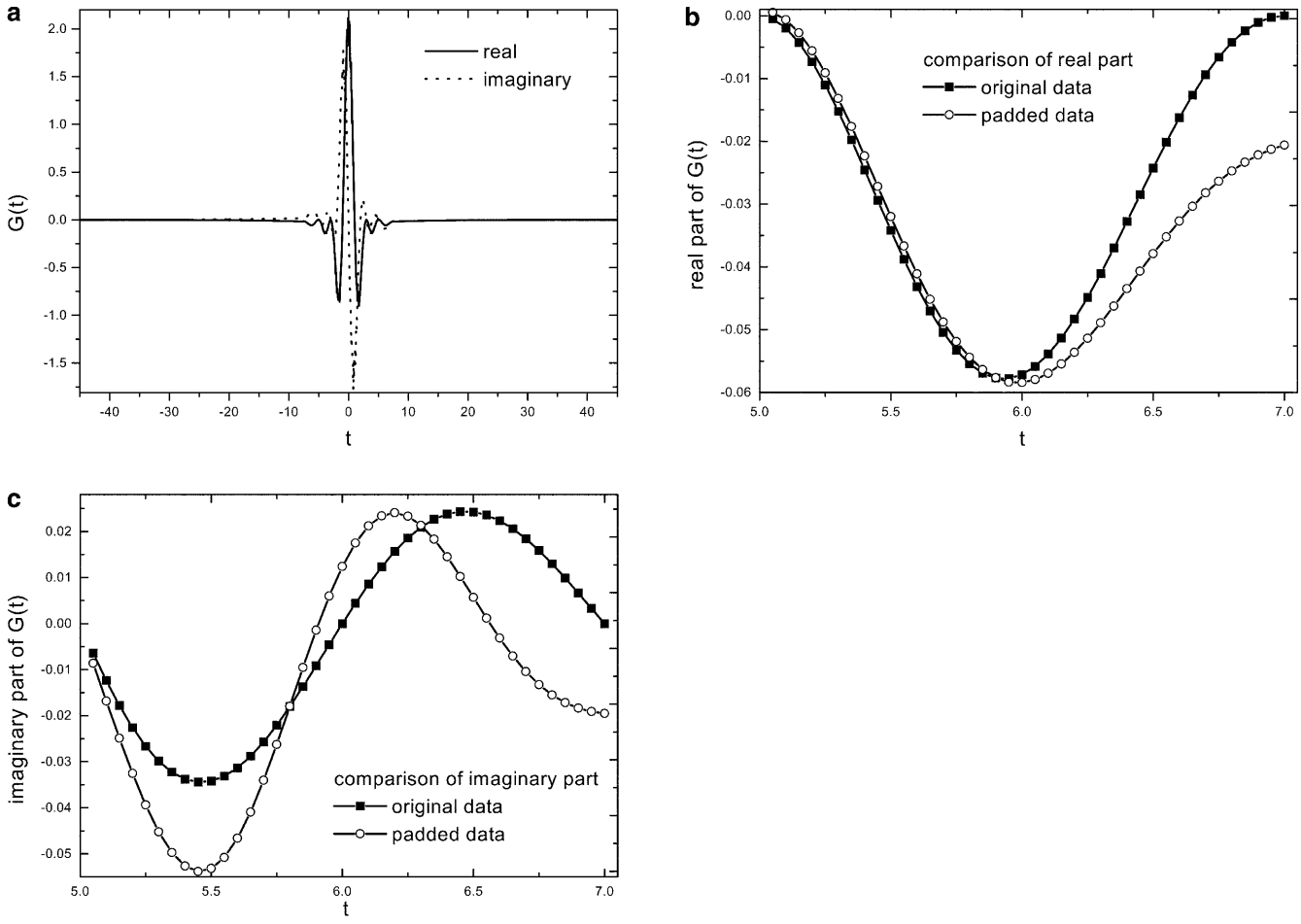

Fig. 15. **a** Time signal (DAF padding 20% noise-corrupted signal). **b** Real parts comparison of original and padded data in noise-corruption case. **c** Imaginary parts comparison of original and padded data in noise-corruption case

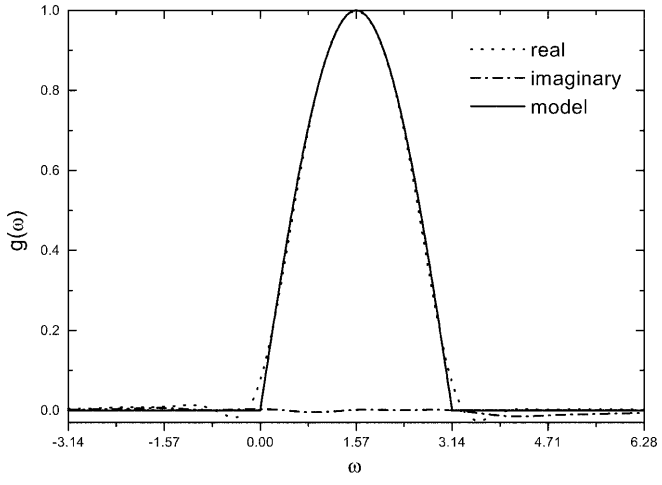

Fig. 16. Spectrum by DPI with DAF padding 20% noise-corrupted signal [DAF parameter $M = 6$, $\sigma(0)/\Delta = 10$]

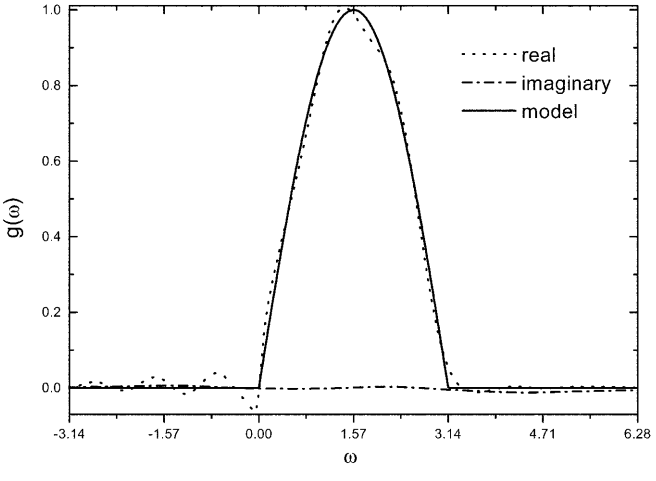

Fig. 17. Spectrum by Fourier transform (DAF padding 20% noise-corrupted signal)

conclude that the traditional Fourier transform is not as robust with respect to noise and padding for a given long-range signal. By contrast, the DPI continues to yield the information contained in the known short-signal segment and is not highly sensitive to the detailed padding.

4 Conclusion

In this article, we have introduced a new method for numerical inversion of the Fourier transform, which we call the DPI method. The use of the DPI is illustrated for

a model problem and the results are compared with the spectrum obtained by the Fourier transform. Our results show that the DPI is more robust than the Fourier transform. In addition, the DPI can remove noise with a minimum of distortion to the true signal, in contrast to the Fourier transform, which is more sensitive to distortions in the signal due to noise. The DPI plus DAF padding is effective at denoising and delivering a good spectrum, but it still produces some ringing in the vicinity of the edges of the true or original compact support frequency-domain signal. Significantly better results should be possible in the DPI if one pads to a more realistic long-range tail.

Acknowledgements. D.K.H., D.J.K. and E.P. were supported in part under a grant from the US-Israel Binational Science Foundation. The Ames Laboratory is operated for the Department of Energy by Iowa State University under Contract No. 2–7405-ENG82. H.Z. and D.J.K. were supported under R. A. Welch Foundation Grant E-0608. Z.S. was supported under NSF Grant CHE-9700297. S.L. acknowledges financial support by the Korea Research Foundation (Distinguished Scholars Program D00239).

References

1. Dattagupta S (1987) Relaxation phenomena in condensed matter physics. Academic, New York
2. May V, Kuhn O (2000) Charge and energy transfer dynamics in molecular systems. Wiley VCH, Berlin
3. Rostkier-Edelstein D, Graf P, Nitzan A (1997) J Chem Phys 107: 10470
4. Gertner BJ, Wilson KR, Hynes JT (1989) J Chem Phys 90: 3537
5. Liao J-L, Pollak E (1999) J Chem Phys 111: 7244
6. Rabani E, Krilov G, Berne BJ (2000) J Chem Phys 112: 2605
7. (a) Heller EJ (1981) Acc Chem Res 14: 368; (b) Imre D, Kinsey JL, Sinha A, Krenos J (1984) J Phys Chem 88: 3956; (c) Heller EJ, Sundberg RL, Tannor D (1982) J Phys Chem 86: 1882; (d) Lee S-Y, Heller EJ (1979) J Chem Phys 71: 4777
8. (a) Feit MD, Fleck JA, Steiger A (1982) J Comput Phys 47: 412; (b) Heller EJ, Stechel EB, Davis MJ (1980) J Chem Phys 73: 4720
9. (a) Gallicchio E, Berne BJ (1994) J Chem Phys 101: 9909; (b) Gallicchio E, Berne BJ (1996) J Chem Phys 105: 7064
10. Wall MR, Neuhauser D (1995) J Chem Phys 102: 8011
11. Mandelshtam VA, Taylor HS (1997) J Chem Phys 106: 5085
12. (a) Hoffman DK, Arnold M, Kouri DJ (1993) J Phys Chem 97: 1110; (b) Kouri DJ, Hoffman DK (1992) In: Broeckhove J, Lathouwers L (eds) Time-dependent Quantum molecular dynamics. Plenum, New York, pp 117–129
13. Nussbaumer HJ (1982) Fast Fourier transform and convolution algorithms. Springer, Berlin Heidelberg New York
14. Beigham EO (1974) Fast Fourier transform. Prentice-Hall, Englewood Cliffs
15. (a) Neuhauser D (1990) J Chem Phys 93: 2611; (b) Neuhauser D (1994) J Chem Phys 100: 5067
16. (a) Mandelshtam VA, Taylor HS (1997) Phys Rev Lett 78: 3274; (b) Mandelshtam VA, Taylor HS (1997) J Chem Phys 107: 6756
17. Zhang DS, Kouri DJ, Hoffman DK, Gunaratne GH (1999) Comput Phys Commun 120: 1
18. (a) Hoffman DK, Nayar N, Sharafeddin OA, Kouri DJ (1991) J Phys Chem 95: 8299 (1991); (b) Kouri DJ, Zhu W, Ma X, Pettitt BM, Hoffman DK (1992) J Phys Chem 96: 9631; (c) Hoffman DK, Kouri DJ (1995) In: Cohen G (ed) Proceedings of the 3rd International Conference on Mathematical and Numerical Aspects of Wave Properties. SIAM, Philadelphia, Pa, pp 56–83
19. Oppenheim AV, Schafer RW (1975) Digital signal processing. Prentice-Hall, Englewood Cliffs